Available online at www.sciencedirect.com
SCIENCE DIRECT
Journal of the European Ceramic Society 26 (2006) 1767–1773
www.elsevier.com/locate/jeurceramsoc

Structure and dielectric properties of perovskite ceramics in the system $Ba(Ni_{1/3}Nb_{2/3})O_3$–$Ba(Zn_{1/3}Nb_{2/3})O_3$

M. Barwick, F. Azough, R. Freer *

Materials Science Centre, School of Materials, University of Manchester, UMIST, Grosvenor Street, Manchester M1 7HS, UK

Available online 14 October 2005

Abstract

Ceramics in the system $Ba(Ni_{1/3}Nb_{2/3})O_3$–$Ba(Zn_{1/3}Nb_{2/3})O_3$ (BNN–BZN) were prepared by the mixed oxide route. Powders were mixed and milled, calcined at 1100–1200 °C then pressed and sintered at temperatures in the range 1400–1500 °C for 4 h. Selected samples were annealed or slowly cooled after sintering. Most products were in excess of 96% theoretical density. X-ray diffraction confirmed that all specimens were ordered to some degree and could be indexed to hexagonal geometry. Microstructural analysis confirmed the presence of phases related to $Ba_5Nb_4O_{15}$ and $Ba_8Zn_1Nb_6O_{24}$ at the surfaces of the samples. The end members BNN and BZN exhibited good dielectric properties with quality factor (Qf) values in excess of 25,000 and 50,000 GHz, respectively, after rapid cooling at 240 °C h^{-1}. In contrast, mid-range compositions had poor Qf values, less than 10,000 GHz. However, after sintering at 1450 °C for 4 h and annealing at 1300 °C for 72 h, specimens of $0.35(Ba(Ni_{1/3}Nb_{2/3})O_3)$–$0.65(Ba(Zn_{1/3}Nb_{2/3})O_3)$ exhibit good dielectric properties: τ_f of +0.6 ppm $°C^{-1}$, relative permittivity of 35 and quality factor in excess of 25,000 GHz. The improvement in properties after annealing is primarily due to an increase in homogeneity.

Keywords: Dielectric properties; Perovskites; Niobates

1. Introduction

Complex perovskite dielectric ceramics are good candidate materials for microwave frequency applications. Ta-based systems, such as $Ba(Zn_{1/3}Ta_{2/3})O_3$ (BZT) and $Ba(Mn_{1/3}Ta_{2/3})O_3$ (BMT) are widely used due to their high relative permittivity (ε_r), quality factor (Qf) and low temperature coefficient of resonant frequency (τ_f).[1,2] The high cost of Ta oxides has called for research of other similar, low-cost materials, such as analogous Nb-based systems.

$Ba(Ni_{1/3}Nb_{2/3})O_3$ and $Ba(Zn_{1/3}Nb_{2/3})O_3$ are cubic perovskite ceramics with spacegroup P_{m3m}. The ordered form of the material introduces lower symmetry, and the system can be indexed as a hexagonal structure (spacegroup P_{-3m1}). A transition from the ordered to the disordered state has been observed in BNN at temperatures above 1400 °C[3–8] and in BZN at above 1300 °C.[6,9] The majority of the previous studies attribute this to the formation of a liquid phase at the grain boundary at and above the transition temperature. As a result, defect concentrations in the grain boundaries are higher, resulting in disorder in the lattice. The order–disorder transitions were found to be coincident with transitions in the lattice parameters. The amount of secondary phase increases with sintering temperature, and also with sintering time above 1500 °C, signifying an increase in the extent of liquid-phase formation during sintering. The increase in the amount of liquid phase and subsequent lattice imperfections at higher temperatures reduces the degree of ordering. In contrast, where homogeneous calcined powders have been used, liquid-phase sintering does not occur and the degree of ordering increases with increasing sintering temperature.[3] However, it has been shown that remnants of this liquid phase, which remains as an intergranular second phase, can dissolve back into the primary material during annealing.[10] Some investigations have also identified NiO-based inclusions in BNN due to unreacted starting materials, emphasising the importance of ensuring homogeneity after calcination.

These findings are consistent with other studies that have taken a "first principles" approach to predicting the order–disorder transition.[11,12] However, the calculated transition temperatures are higher than the experimentally determined values. This difference was attributed to the inability of the theoretical model to account for inhomogeneity and liquid-phase sintering. Noh et al.[13] showed that the quality factor increases with sintering temperature and time up to the transition temperature,

* Corresponding author. Tel.: +44 161 306 3564; fax: +44 161 306 8877.
E-mail address: Robert.Freer@manchester.ac.uk (R. Freer).

0955-2219/$ – see front matter © 2005 Elsevier Ltd. All rights reserved.
doi:10.1016/j.jeurceramsoc.2005.09.004

although the degree of ordering did not vary significantly. The large improvements seen in Qf values have been attributed to the higher densities and larger grain sizes brought about by liquid-phase sintering.[13]

The high volatility of Zn and Ni introduces further complications. The longer sintering and/or annealing times required to improve the degree of ordering encourage the loss of these species from the material during processing. This leads to a surface region rich in barium niobate.[14]

In the system BNN–BZN, compositions with τ_f of (or near) zero can be achieved, but sometimes at the cost of other properties. Ceramics of 0.7BNN–0.3BZN sintered at 1500 °C have been reported to have a zero temperature coefficient of resonant frequency with an acceptably high quality factor.[15] However, this does not give the highest possible Qf value. As with the majority of perovskite ceramics, small variations in the processing condition have marked effects on the properties. The temperature-stable composition can vary depending on the processing conditions. For example, Lee et al.[16] prepared a 0.4BNN–0.6BZN composition with a zero τ_f. This apparent discrepancy can be attributed to variations in the processing routes, as well as the nature of the starting materials and the homogeneity of the sintered products.

The focus of the present study is the $Ba(Ni_{1/3}Nb_{2/3})O_3$–$Ba(Zn_{1/3}Nb_{2/3})O_3$ system. The effect of the processing route on the physical and dielectric properties has been investigated, addressing in particular, the sintering temperatures, cooling rates and annealing times, with a view to producing a temperature-stable material with a high relative permittivity and Qf, suitable for use as a low-cost microwave dielectric ceramic.

2. Experimental

Samples were produced via the mixed-oxide route. High purity oxides $BaCO_3$, NiO, ZnO and Nb_2O_5 were mixed in appropriate proportions and vibro-milled with propan-2-ol and zirconia milling media for 24 h (B_2O_3 was added to BNN to improve sinterability). After drying, the powders were calcined at 1100–1200 °C for 4 h, then milled as before and dried. Batches of powder (10 g) were uniaxially pressed in a steel die to form disc-shaped pellets. For sintering, the samples were placed on powder of the same composition on an alumina plate and covered with an alumina crucible to minimise loss of volatile species. Sintering was performed in a Vecstar VF1 chamber furnace at temperatures in the range 1400–1500 °C for 4 h. Standard heating and cooling rates were 240 °C h^{-1}. Selected samples were cooled at slower rates (down to 2 °C h^{-1}) and annealed at 1300 °C for times up to 72 h. Fired densities were determined from weight and dimension measurements.

Sintered samples were ground on SiC down to 1200 grade and polished using 6 and 1 μm diamond paste. A thermal etch at 1100 °C was sufficient to reveal the microstructure. The samples were examined using a Phillips XL30 FEG scanning electron microscope. A Philips SEM525 EDAX DX4 scanning electron microscope was used for EDX analysis. For X-ray diffraction analysis, polished and as-sintered samples were cut to size using a diamond-tipped saw and then examined by a Philips PW1877 employing Cu Kα1 radiation. Samples were scanned from 10 to 110° 2θ in a continuous mode at 0.008° 2θ s^{-1}. Lattice parameters were derived from the diffraction data. The degree of ordering was determined by comparing the hexagonal (1 0 0) peak to the (1 1 0, 0 1 2, 1 0 2) peak. Dielectric loss and relative permittivity were determined by the Hakki-Coleman (parallel plate) method[17] in association with an HP 8720ET network analyser. The temperature coefficient of resonant frequency (τ_f) was determined using a silver-plated aluminium cavity over the temperature range −10 to 60 °C.

3. Results and discussion

From Fig. 1 it can be seen that density generally increases with increasing sintering temperature. This is attributed primarily to the increased level of diffusion at high temperatures. For BZN, maximum density was achieved at sintering temperatures of 1450–1475 °C, whilst for the other end member, BNN, the optimum sintering temperature was 1475 °C. At these temperatures, densities in excess of 96% theoretical were achieved. Reducing the cooling rate after sintering from 240 to 2 °C h^{-1} caused nonlinear variation in density (Fig. 2). For both BZN and BNN the density initially reduced as cooling rate became slower, but there was a slight increase in density for cooling rates in the range 30–10 °C h^{-1} (Fig. 2). This was followed by a reduction

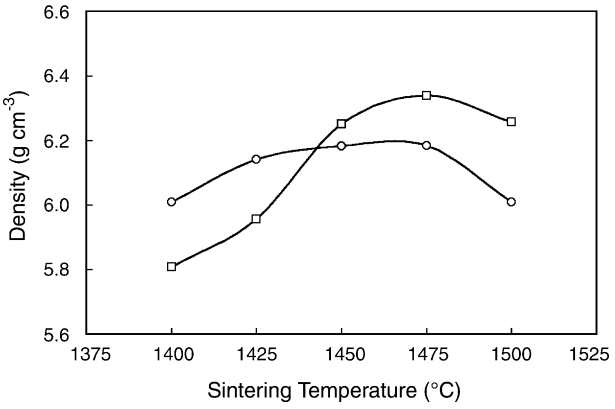

Fig. 1. Density as a function of sintering temperature for BNN (□) and BZN (○).

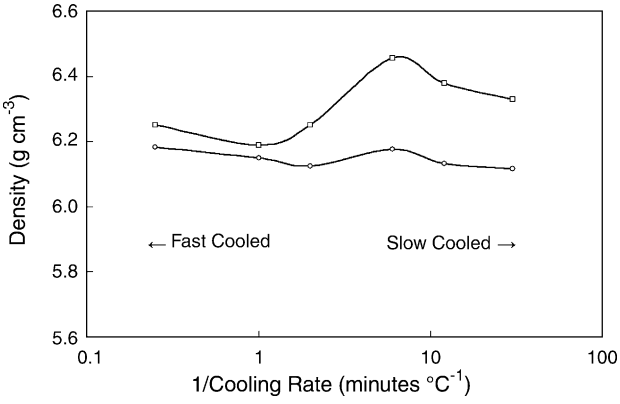

Fig. 2. Density as a function of postsinter cooling rate for BNN (□) and BZN (○).

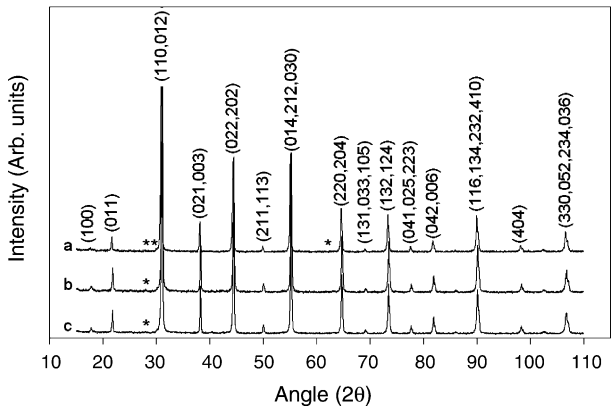

Fig. 3. X-ray diffraction spectra for BNN ceramics sintered at (a) 1500 °C, (b) 1450 °C and (c) 1400 °C for 4 h. Peaks from impurity phases are marked with asterisks (*).

in density. The changes reflect competition between enhanced densification (achieved by the slower cooling rate, i.e. longer time spent at higher temperature) and loss of volatile species. Similarly, annealing at 1300 °C (for times up to72 h) after sintering, initially led to a reduction in density (upon the loss of volatile species including Zn), but at the longest anneal times, maximum density was achieved. Sample density depends critically on the time the sample spends at elevated temperature and the loss of volatile species.

Typical X-ray diffraction spectra for BNN ceramics sintered at 1400–1500 °C are shown in Fig. 3. The majority of peaks can be indexed according to the hexagonal perovskite structure, although there are very small peaks that are due to secondary surface phases. Very similar behaviour was observed for BZN ceramics and solid solutions. There are marked changes in the lattice parameters for both BNN and BZN when sintered at temperatures above ~1450 °C (the order–disorder transition); Fig. 4. The increase in the cell parameters is due, in part, to the development of inhomogeneity in the structure as the distribution of B^{2+} and B^{5+} ions becomes more random. Kim et al.[9] reported a similar transition for this system, but at lower temperatures. They attributed the transition to the onset of liquid-phase sintering. However, in the present study, there is no evidence for a residual grain boundary phase and extensive mixing and milling ensured minimal inhomogeneity in the calcined powders.

The degree of cation ordering can be quantified in terms of the relative integrated intensity (peak height/peak width at half height) of the (1 0 0) and (1 1 0, 0 1 2, 1 0 2) hexagonal lattice reflections, i.e. $(I_{(1\,0\,0)}/I_{(1\,1\,0,\,0\,1\,2,\,1\,0\,2)})_{\mathrm{obs}}$ for the experimental data. By comparing this with a calculated value for a fully ordered material, the ordering parameter, S, can be defined by Eq. (1),

$$S = \sqrt{\frac{(I_{100}/I_{110,012,102})_{\mathrm{obs}}}{(I_{100}/I_{110,012,102})_{\mathrm{calc}}}} \quad (1)$$

where $(I_{(1\,0\,0)}/I_{(1\,1\,0,\,0\,1\,2,\,1\,0\,2)})_{\mathrm{calc}}$ is the calculated relative integrated intensity of the (1 0 0) and the (1 1 0, 0 1 2, 1 0 2) peaks.[7] Fig. 4c shows the ordering parameter (S) and lattice parameter aspect ratio (c/a) as a function of sintering temperature. It can be

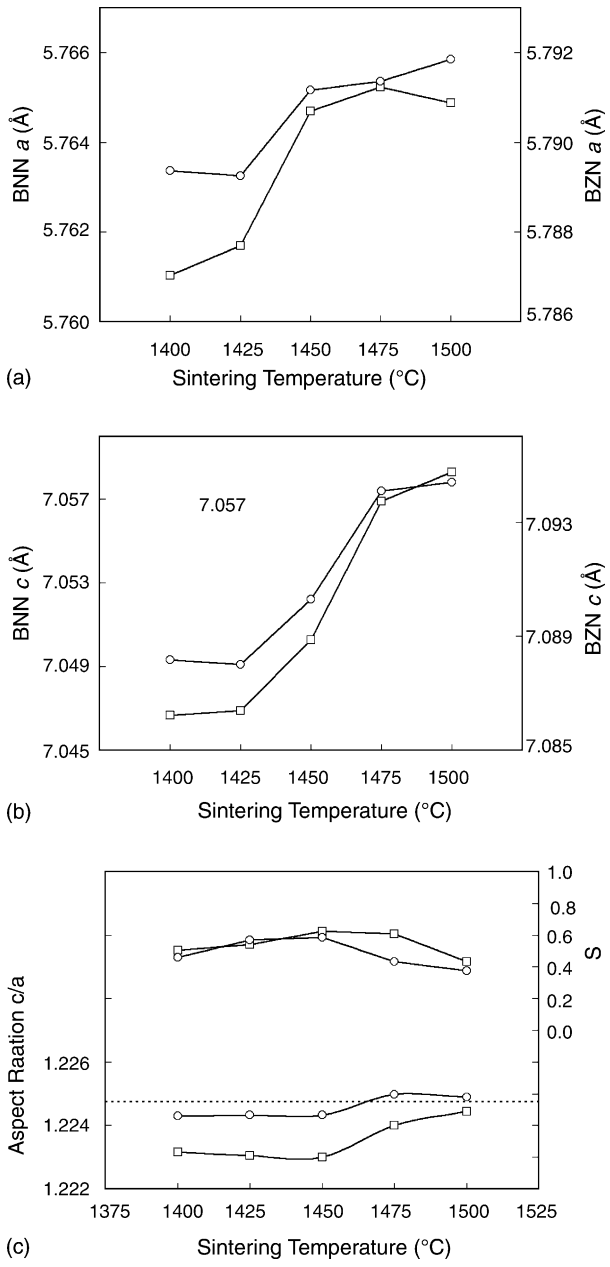

Fig. 4. (a) The hexagonal lattice parameter a as a function of sintering temperature for BNN (□) and BZN (◯). (b) The hexagonal lattice parameter c as a function of sintering temperature for BNN (□) and BZN (◯). (c) Ordering parameter (S) and unit cell aspect ratio (c/a) as a function of sintering temperature for BNN (□) and BZN (◯). The dashed line shows the ideal aspect ratio, $\sqrt{3}/\sqrt{2}$ (values above this show elongation in the c direction).

seen that S increases with sintering temperature, but exhibits a transition in behaviour and sudden decrease at 1475 °C for BNN and at 1450 °C for BZN. This is consistent with the changes in the lattice parameters (Fig. 4a and b). As the order parameter is based on the measurement of a very low-intensity peak, the actual lattice parameters are more reliable indicators of the transition temperature. However, an increase in lattice parameters may also be brought about by an increase in defect concentration, or possibly incorporation of impurities into the host structure. The anisotropy of the crystal structure can be characterised in

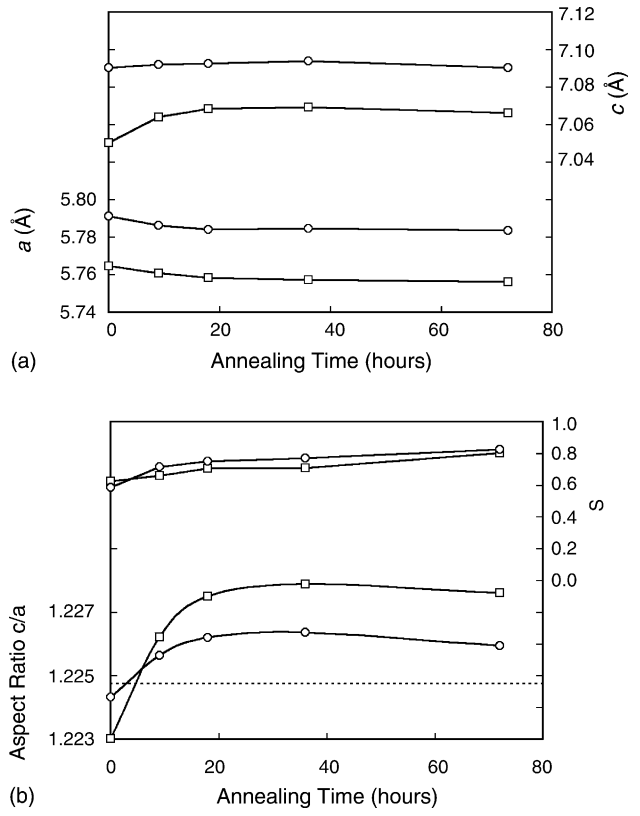

Fig. 5. (a) The hexagonal lattice parameters as a function of annealing time at 1300 °C for BNN (□) and BZN (◯). (b) Ordering parameter (S) and unit cell aspect ratio (c/a) as a function of annealing time at 1300 °C for BNN (□) and BZN (◯). The dashed line shows the ideal aspect ratio, $\sqrt{3}/\sqrt{2}$ (values above this show elongation in the c direction).

terms of the unit cell aspect ratio, c/a, which is also shown in Fig. 4c. There is a clear increase in the aspect ratio for sintering temperatures of 1450–1475 °C, reflecting the structural transition temperatures.

Changes in structural parameters were also recorded when samples were annealed at constant temperature after sintering (Fig. 5). As annealing time increases, the hexagonal lattice parameter a, for both BNN and BZN decreases, whereas the c dimension initially increases and then decreases (Fig. 5a). Fig. 5b shows that the order parameter (S) increases and approaches the fully ordered state (i.e. $S \rightarrow 1$), as annealing time increases; the improvement in S being marginally higher for BZN than BNN. When the sample is held at 1300 °C, well below the order–disorder transition, the ordering improves, but the rate of increase reduces as annealing time increases. The elongation of the unit cell in the c direction during the initial stage of annealing corresponds to the rapid improvement in S. The distortion in the cell is reduced as the rate of change of the order parameter decreases and a fully ordered structure evolves. The same trends are also seen for studies as a function of postsinter cooling rate. With slower cooling, the S values initially decrease, but at very slow cooling rates the level of order improves dramatically. The variation in unit cell aspect ratio is similar; lower cooling rates lead to an initial elongation in the c direction and a general decrease in unit cell volume, with the greatest distortion again occurring where the order parameter changes most rapidly.

This goes some way to establishing a link between the unit cell aspect ratio and the degree of order. The onset of the ordering mechanism during annealing involves elongation in the c direction. In contrast, the partially ordered structure brought about by sintering below the transition temperature involves elongation in the a direction.

In contrast to previous findings,[3,6,9,10,13,18] there was no evidence of any intergranular impurity phases within the bulk material of the sample. However, EDS analysis confirmed that both BNN and BZN contain the phase $Ba_5Nb_4O_{15}$ at the sample surface (Fig. 6). The BZN also shows a third phase, nominally $Ba_8(ZnNb_6)O_{24}$, between the primary and surface phases (Fig. 6b). This is analogous to the impurity phase recently found in BZT.[19,20] The $Ba_8(ZnNb_6)O_{24}$ is a perovskite-type structure, with regular stacking faults, giving recurrent planes of face-sharing (as opposed to corner-sharing) oxygen octahedra. This is thought to compensate for the Zn vacancies resulting from the lost material during processing. Mixed samples of BNN–BZN also show the $Ba_5Nb_4O_{15}$ surface phase, plus a clear third phase between the bulk stoichiometric perovskite and the surface phase (Fig. 6c). This third phase has similar stoichiometry to the $Ba_5Nb_4O_{15}$ phase, but contains discernable levels of Ni. This suggests that Zn is more readily lost than Ni from the samples during processing. EDS examination of the bulk microstructure of the solid-solution samples revealed isotropic grains of two distinct compositions: BNN with low levels of Zn and BZN with low levels of Ni. The distribution of these grains was random throughout the sample, but the relative amounts of constituent species were consistent with solid-solution composition. This can be attributed to the processing route, where precalcined powders of each end member were mixed and milled prior to sintering, as opposed to sintering a calcined $Ba([Ni_xZn_{1-x}]_{1/3}Nb_{2/3})O_3$ composition. Annealed or slow cooled samples showed a more homogeneous compound, implying greater interdiffusion of the B-site species between the constituent grains. The variation in grain size closely followed the trends in density, generally increasing with higher sintering temperature, longer annealing time and slower cooling rates. The time the sample spends at higher temperature enables further diffusion and therefore, increased grain growth. The lack of any obvious transitions in grain size and/or density with variations in processing conditions supports the proposal of a sintering mechanism that does not involve a liquid phase.

Fig. 7 shows the dielectric quality factor, relative permittivity and temperature coefficient of resonant frequency as a function of compositions in the xBNN–$(1-x)$BZN solid-solution system for $0<x<1$. Ceramics with composition 0.35BNN–0.65BZN exhibited a near-zero τ_f. This supports the findings of previous studies, although earlier investigations have indicated compositions ranging from 0.7BNN–0.3BZN to 0.4BNN–0.6BZN.[15,16] The relative permittivity decreases approximately linearly with composition from BZN ($\varepsilon_r \sim 40$) to BNN ($\varepsilon_r \sim 26$), reflecting a simple composition–volume relationship. Whilst the quality factors of the end members are in excess of 20,000, particularly BZN (~50,000), the mid-

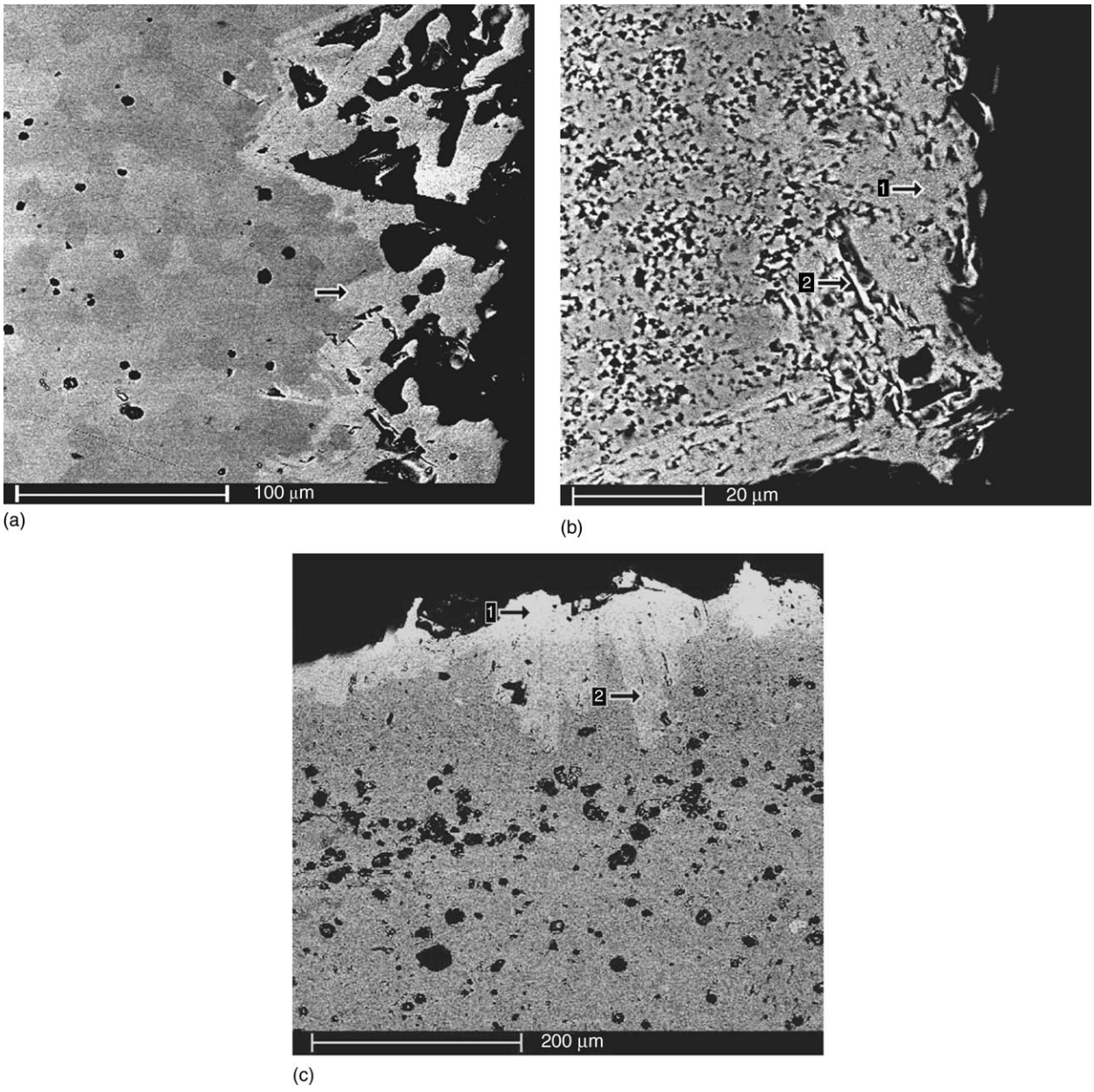

Fig. 6. (a) Backscattered electron micrograph of the edge region of a BNN sample. The $Ba_5Nb_4O_{15}$ surface phase is identified by arrow. (b) Backscattered electron micrograph of the edge region of a BZN sample. The $Ba_5Nb_4O_{15}$ surface phase is identified by arrow 1; the $Ba_8(ZnNb_6)O_{24}$ perovskite-type phase is identified by arrow 2. (c) Backscattered electron micrograph of the edge region of an annealed BNN–BZN solid-solution sample. The $Ba_5Nb_4O_{15}$ surface phase is identified by arrow 1; the $Ba_5Nb_4O_{15}$-type phase (containing low levels of Ni) is identified by arrow 2.

range compositions ($0.2 < x < 0.9$) exhibit very poor Qf values (<10,000). This trend mirrors the behaviour found in the system $Ba(Ni_{1/3}Nb_{2/3})O_3$–$Ba(Co_{1/3}Nb_{2/3})O_3$ (BNN–BCN) by Ahn et al.[21] Depending upon the processing route, the Qf generally follows the same trends as *S*, indicating that the Qf value is strongly dependent on ordering. This is usually at the cost of the relative permittivity, which tends to decrease as *S* rises. However, the change in ε_r is negligible in comparison to the vast improvements of Qf. Where the Qf values deviate from the simple ordering trend, i.e. for mixed BNN–BZN composition, Qf may be improved by increasing the density and reducing the influence of extrinsic factors on the loss characteristics. Annealing brings about the greatest improvement in Qf. Slow cooling rates can also improve Qf values, but the final behaviour and properties also depend on the amount and type of surface phases generated. The primary surface phase $Ba_5Nb_4O_{15}$ exhibits properties that make it potentially suitable for use as a microwave dielectric. However, its presence as a second phase, greatly reduces the Qf values of BZN–BNN ceramics. It is clearly the interaction between this phase and the bulk perovskite that has an impact on the Qf. Investigation of the near-zero τ_f composition (0.35BNN–0.65BZN) has shown that the low-quality factor can be improved by annealing (Fig. 8). This suggests that the interdiffusion of Ni and Zn in the initially distinct grains

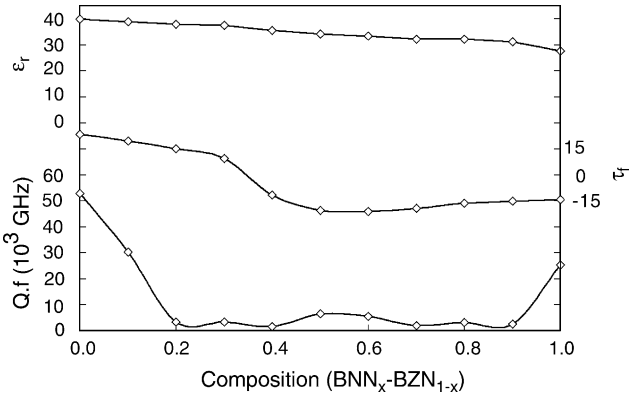

Fig. 7. Relative permittivity, temperature coefficient of resonant frequency and Qf values for the BNN_x–BZN_{1-x} system (samples sintered at 1450 °C for 4 h).

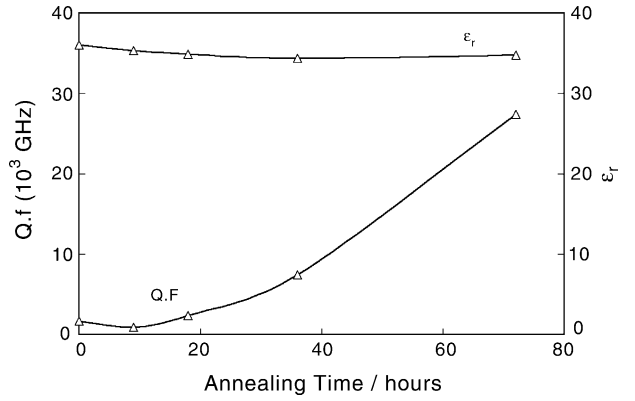

Fig. 8. Relative permittivity and Qf values for 0.35BNN–0.65BZN ceramic as a function of annealing time at 1300 °C (after sintering for 4 h at 1450 °C).

and hence increased homogeneity greatly reduces the dielectric loss. Furthermore, detailed kinetic studies of ordering suggest that BNN and BZN order at significantly different rates. This reflects the differing mobility of Zn and Ni in the perovskite lattice.

4. Conclusions

Small variations in the processing route can have a significant impact on the dielectric properties of niobate perovskites. High sintering temperatures improve densification but at the cost of the degree of cation order. Annealing and slow cooling improves the Qf values, but the slower cooling rates lead to an increase in the amount of surface secondary phase, which is detrimental to the Qf.

The composition $0.35(Ba(Ni_{1/3}Nb_{2/3})O_3)$–$0.65(Ba(Zn_{1/3}Nb_{2/3})O_3)$ sintered at 1450 °C for 4 h and annealed for 72 h at 1300 °C exhibits good dielectric properties: τ_f of +0.6 ppm °C^{-1}, relative permittivity of 35 and quality factor in excess of 25,000 GHz. The improvement in quality factor following annealing can be attributed to the increased homogeneity of the solid solution after diffusion of Ni and Zn within the bulk material. This makes the ceramic suitable for microwave dielectric applications.

Acknowledgements

The provision of an EPSRC Doctoral Training Award (to M.B.), the financial support of EPSRC through GR/R72655/01 and the assistance of Filtronic Ltd. with microwave measurements are gratefully acknowledged.

References

1. Klein, N., Schuster, M., Vitusevich, S., Winter, M. and Yi, H. R., Novel dielectric resonator structures for future microwave communication systems. *J. Eur. Ceram. Soc.*, 2001, **21**, 2687–2691.
2. Tamura, H., Konoike, T., Sakabe, Y. and Wakino, K., Improved high-Q dielectric resonator with complex perovskite structure. *J. Am. Ceram. Soc.*, 1984, **67**, C59–C61.
3. Kim, I. T., Kim, Y. H. and Chung, S. J., Order–disorder transition and microwave dielectric-properties of $Ba(Ni_{1/3}Nb_{2/3})O_3$ ceramics. *Jpn. J. Appl. Phys.*, 1995, **1**(34), 4096–4103.
4. Kim, B. K., Hamaguchi, H., Kim, I. T. and Hong, K.-S., Probing of 1:2 ordering in $Ba(Ni_{1/3}Nb_{2/3})O_3$ and $Ba(Zn_{1/3}Nb_{2/3})O_3$ ceramics by XRD and Raman spectroscopy. *J. Am. Ceram. Soc.*, 1995, **78**, 3117–3120.
5. Kim, I. T., Kim, Y. H. and Chung, S. J., Ordering and microwave dielectric properties of $Ba(Ni_{1/3}Nb_{2/3})O_3$ ceramics. *J. Mater. Res.*, 1997, **12**, 518–525.
6. Hong, K.-S., Kim, I. T. and Kim, C. D., Order–disorder phase formation in the complex perovskite compounds $Ba(Ni_{1/3}Nb_{2/3})O_3$ and $Ba(Zn_{1/3}Nb_{2/3})O_3$. *J. Am. Ceram. Soc.*, 1996, **79**, 3218–3224.
7. Kolodiazhnyi, T., Petric, A., Belous, A., V'yunov, O. and Yanchevskij, O., Synthesis and dielectric properties of barium tantalates and niobates with complex perovskite sturcture. *J. Mater. Res.*, 2002, **17**, 3182–3189.
8. Banno, H., Mizuno, F., Takeuchi, T., Tsunooka, T. and Ohya, K., Dielectric properties of $Sr(Ni_{1/3}Nb_{2/3})O_3$-$Ba(Ni_{1/3}Nb_{2/3})O_3$ ceramics at microwave frequencies. *Jpn. J. Appl. Phys.*, 1985, **24**, 87–89.
9. Kim, I. T., Hong, K.-S. and Yoon, S. J., Effects of non-stoichiometry and chemical inhomogeneity on the order–disorder phase formation in the complex perovskite compounds, $Ba(Ni_{1/3}Nb_{2/3})O_3$ and $Ba(Zn_{1/3}Nb_{2/3})O_3$. *J. Mater. Sci.*, 1995, **30**, 514–521.
10. Park, J.-K., Kim, D.-Y. and Yoon, D. Y., Discontinuous dissolution of a liquid phase in $Ba(Ni_{1/3}Nb_{2/3})O_3$ ceramics. *J. Am. Ceram. Soc.*, 2001, **84**, 218–220.
11. Bellaiche, L., Padilla, J. and Vanderbilt, D., Heterovalent and A-atom effects in $A(B'B'')O_3$ perovskite alloys. *Phys. Rev. B*, 1999, **59**, 1834–1839.
12. Takahashi, T., First-principles investigation of the phase stability for $Ba(B_{1/3}'^{2+}B_{2/3}''^{5+})O_3$ microwave dielectrics with the complex perovskite structure. *Jpn. J. Appl. Phys.*, 2000, **39**, 5637–5641.
13. Noh, S.-Y., Yoo, M. J., Nahm, S., Choi, C. H., Park, H.-M. and Lee, H.-J., Effect of stuctural changes on the microwave dielectric properties of $Ba(Zn_{1/3}Nb_{2/3})O_3$ ceramics. *Jpn. J. Appl. Phys.*, 2002, **41**, 2978–2981.
14. Hughes, H., Iddles, D. and Reaney, I. M., Niobate-based microwave dielectrics suitable for third generation mobile phone base stations. *Appl. Phys. Lett.*, 2001, **79**, 2952–2954.
15. Cho, S. Y., Youn, H. J. and Hong, K. S., A New microwave dielectric ceramic based on the solid-solution system between $Ba(Ni_{1/3}Nb_{2/3})O_3$ and $Ba(Zn_{1/3}Nb_{2/3})O_3$. *J. Mater. Res.*, 1997, **12**, 1558–1562.
16. Lee, J. H., Jang, Y. I., Youn, H. J., Jang, J. W. and Kim, B. K., Low-firing and microwave dielectric properties of $Ba[(Ni_{0.6}Zn_{0.4})_{0.33}Nb_{0.67}]O_3$ ceramics doped with Sb_2O_5 and B_2O_3. *J. Mater. Sci.*, 1999, **34**, 625–628.
17. Hakki, B. W. and Coleman, P. D., A dielectric resonator method of measuring inductive capacities in the millimeter range. *IEEE Trans. Microw. Theory Tech.*, 1960, **8**, 402–410.

18. Kim, I. T., Chung, S. J. and Hong, K.-S., Effects of liquid phase formation on the order–disorder behaviour of $Ba(Ni_{1/3}Nb_{2/3})O_3$. *Ferroelectrics*, 1995, **173**, 125–137.
19. Bieringer, M., Moussa, S. M., Noailles, L. D., Burrows, A., Kiely, C. J., Rosseinsky M. J., *et al.*, Cation ordering, domain growth and zinc loss in the microwave dielectric oxide $Ba_3ZnTa_2O_9$-δ. Chem. Mater., 2003, **15**, 586–597.
20. Davies, P. K., Borisevich, A. and Thirumal, M., Communicating with wireless perovskites: cation order and zinc volatilisation. J. Eur. Ceram. Soc., 2003, **23**, 2461–2466.
21. Ahn, C.-W., Jang, H.-J., Nahm, S., Park, H.-M. and Lee, H.-J., Effects of microstructure on the microwave dielectric properties of $Ba(Co_{1/3}Nb_{2/3})O_3$ and $(1-x)Ba(Co_{1/3}Nb_{2/3})O_3$–$xBa(Zn_{1/3}Nb_{2/3})O_3$ ceramics. *J. Eur. Ceram. Soc.*, 2003, **23**, 2473–2478.